The Theoretical Basis of the Kinetic Method from the Point of View of Finite Heat Bath Theory

Julia Laskin* and Jean H. Futrell

Pacific Northwest National Laboratory, William R. Wiley Environmental Molecular Sciences Laboratory, P.O. Box 999 (K8-96), Richland, Washington 99352

Received: April 24, 2000; In Final Form: July 20, 2000

We present a rigorous theoretical basis of the kinetic method, commonly used for thermochemical determinations in mass spectrometry, based on finite heat bath theory (FHBT) developed by Klots. A simple analytical expression for the branching ratio is derived from FHBT formalism. This expression simplifies to the expression given by the absolute reaction rate theory (1) for very large clusters or (2) for reactions having a negligible kinetic shift. The reacting population is described by two different temperatures rather than by the "effective" temperature as suggested previously. Simulations performed using both RRKM and FHBT revealed that the kinetic plots are slightly nonlinear. The observed curvature is related to the changes in the transition state temperature as a function of the critical energy for fragmentation. The curvature of the plots decreases for larger clusters. We show that the "effective" temperature closely resembles the average value of the transition state temperature. This allows us to assign a new definition of the effective temperature and predict its properties. The results of simulations confirm that the extended version of the kinetic method introduced by Fenselau and co-workers provides accurate relative energetics for competitive reactions for both small and large ions. However, accurate thermochemical information can be obtained from the kinetic method only if reactions under investigation have negligible reverse activation energies. A new approach for extracting relative fragmentation energetics and entropy differences for two competing reactions is proposed. This approach requires a measurement of kinetic energy release distributions (KERDs) for the two fragmentation channels; the relative energetics and dynamics can be extracted from a *single* measurement.

Introduction

The gas-phase basicity (GB) and the proton affinity (PA) are defined as the negative of the free energy change ($-\Delta G$) and the enthalpy change ($-\Delta H$), respectively, for the reaction

$$B_{(g)} + H_{(g)}^{+} \rightarrow BH_{(g)}^{+} \qquad (1)$$

Experimental methods used to determine these important thermochemical properties comprise equilibrium measurements, threshold measurements, the bracketing method, and the kinetic method. The basic assumptions of the above methods, their limitations and applications to numerous chemical systems, have been extensively reviewed[1−4] and will not be discussed here.

The kinetic method introduced by Cooks and co-workers[5,6] is probably the most widely used mass spectrometric method for thermochemical determinations. The kinetic method is particularly attractive because it is (1) easy to use (can be implemented on any tandem mass spectrometer); (2) can be applied to nonvolatile and thermally labile species; (3) is sensitive to small differences in thermochemical properties, and (4) does not require any theoretical modeling. As a result, this method has been used for acquiring information on the *relative* values of various thermochemical quantities including proton and electron affinities, ionization energies, metal ion affinities, and heterolytic bond dissociation energies of a wide variety of molecules.[1−3]

* Corresponding author. E-mail: Julia.Laskin@pnl.gov. Fax: (509) 3763650.

The relative proton affinity and the gas-phase basicity of a molecule (B_1) are evaluated by monitoring the branching ratio upon fragmentation of a proton bound dimer $[B_1-H^+-B_2]$

$$[B_1 - H^+ \text{ -- } B_2] \xrightarrow{k_1} B_2 + B_1H^+ \qquad (2a)$$

$$[B_1 - H^+ \text{ -- } B_2] \xrightarrow{k_2} B_2H^+ + B_1 \qquad (2b)$$

where B_2 is a reference base with known proton affinity. Two monomers composing the dimer will compete for the proton based on their relative proton affinities. It follows that the difference in proton affinities of B_1 and B_2 will be reflected in the experimentally measured branching ratio $[B_1H^+]/[B_2H^+]$. From the absolute reaction rate theory the branching ratio can be expressed as follows:

$$\ln\left(\frac{[B_1H^+]}{[B_2H^+]}\right) = \ln\left(\frac{k_1}{k_2}\right) = \ln\left(\frac{Q_1^{\ddagger}}{Q_2^{\ddagger}}\right) + \frac{PA(B_1) - PA(B_2)}{RT_{eff}} \qquad (3)$$

where $Q_1^{\ddagger}$ and $Q_2^{\ddagger}$ refer to the partition functions of the transition states of the two competing dissociation channels, T_{eff} is the so-called "effective" temperature that is defined as the temperature of the canonical ensemble for which fragmentation would yield the same branching ratio as observed experimentally, and

$$PA(B_1) - PA(B_2) = \Delta H_2 - \Delta H_1 = \Delta E_2 - \Delta E_1$$

where ΔH_1, ΔE_1 and ΔH_2, ΔE_2 are the enthalpy and the critical

10.1021/jp001556b CCC: $19.00
Published on Web 09/02/2000

energy for reactions 2a and 2b, respectively. Equation 3 is valid (1) for the system in thermal equilibrium and (2) assuming that reactions 2a and 2b have negligible reverse activation energies.

The ratio of the partition functions, $Q_1^{\ddagger}/Q_2^{\ddagger}$, is characteristic of the differences in entropy of the two competing reactions. Equation 3 can be simplified assuming that the entropy effects for reactions 2a and 2b are similar and cancel each other ($Q_1^{\ddagger} = Q_2^{\ddagger}$)

$$\ln\left(\frac{k_1}{k_2}\right) = \frac{\mathrm{PA(B_1)} - \mathrm{PA(B_2)}}{RT_{\mathrm{eff}}} \tag{4}$$

In this case the plot of $\ln(k_1/k_2)$ vs $PA(B_2)$ (the kinetic plot) is a straight line with the slope given by $-1/RT_{\mathrm{eff}}$ and the intercept given by $PA(B_1)/RT_{\mathrm{eff}}$. Therefore the proton affinity of B_1 can be determined from the slope and the intercept of the kinetic plot.

The assumption of similar entropy effects for reactions 2a and 2b used to derive eq 4 is valid if B_1 and B_2 are structurally similar bases. However, eq 4 cannot be used if the fragmentation of a proton-bound dimer composed of structurally dissimilar bases is examined or if one of the products has internal hydrogen bonds. Fenselau and co-workers introduced an important extension of the kinetic method to account for the differences in the entropy effects of reactions 2a and 2b.[7−9] Assuming that $\ln(Q_1^{\ddagger}/Q_2^{\ddagger})$ is constant over the range of effective temperatures sampled experimentally, one obtains

$$\ln\left(\frac{k_1}{k_2}\right) = \frac{\mathrm{PA(B_1)} - \mathrm{PA(B_2)}}{RT_{\mathrm{eff}}} - \frac{\Delta(\Delta S)}{R} \tag{5}$$

where $\Delta(\Delta S) = \Delta S_2^{\ddagger} - \Delta S_1^{\ddagger}$. According to eq 5, the slope of the kinetic plot yields $1/RT_{\mathrm{eff}}$ and the intercept will be given by

$$\text{intercept} = \mathrm{PA(B_1)}/RT_{\mathrm{eff}} - \Delta(\Delta S)/R \tag{6}$$

To obtain information both on the proton affinity of the unknown and $\Delta(\Delta S)$ for reactions 2a and 2b, the branching ratios are measured at different collision energies, corresponding to different effective temperatures. The effective temperatures can be extracted from the slopes of the kinetic plots. The plot of the intercepts obtained from the energy-dependent kinetic plots vs the corresponding slopes will give a straight line, where now the slope and the intercept correspond to the proton affinity, $PA(B_1)$, and the entropy difference for the competing reactions, $\Delta(\Delta S)$, respectively. This approach allows determining of the thermochemical quantities of molecules for which a set of structurally similar reference bases does not exist.[8−12]

The kinetic method has been extensively used to determine proton affinities and gas-phase basicities; most of the proton affinities obtained using this method are within 2 kcal/mol of values obtained using alternative methods.[1,3] However, substantial discrepancies (more than 10 kcal/mol) between the results from the bracketing and the kinetic method were found in determining proton affinities of polyglycines and polyalanines.[2] This result challenges whether the kinetic method is generally capable of providing accurate proton affinities of peptides.

Despite wide use of the kinetic method, its theoretical basis has not been clearly established. Its basic assumptions were examined in several key publications.[4,13−17] The main assumptions are: (1) reactions 2a and 2b have negligible reverse activation barriers; (2) the fraction of ions that undergo fragmentation can be characterized by an effective temperature; (3) the proton bound dimer is a weakly bound complex, and (4) reactions 2a and 2b are the only fragmentation channels observed in the experiment. Furthermore, eqs 4 and 5, employed by the kinetic method, are derived from the absolute reaction rate theory and are rigorously valid only for systems in thermal equilibrium. However, an ensemble of ions undergoing metastable or collision-induced decay in a tandem mass spectrometer cannot be characterized by a thermal distribution of energies.

It has been shown by several groups that eq 4 can be derived from RRK formalism without assuming thermal equilibrium for the ensemble of ions undergoing fragmentation in a mass spectrometer.[18−20] RRKM simulations performed by Brauman and co-workers demonstrated that the branching ratio for competing reactions depends exponentially on the difference in the barrier heights for these reactions ($\Delta\Delta E$).[19] This observation provided a strong support of the validity of eq 4. They further concluded that the exponential behavior of the branching ratio on $\Delta\Delta E$ requires that $\Delta\Delta E$ is small relative to the excess internal energy above the fragmentation threshold. These authors also pointed out that RRKM calculations could not establish that eq 4 should be valid.

Although the validity of use of the effective temperature, T_{eff}, in eqs 4 and 5 has been extensively discussed,[13−15] the physical meaning of the effective temperature remains unclear. This led Holmes and co-workers to suggest discontinuing the use of the term "effective" temperature as having no physical meaning.[15] They also pointed out that the ensemble of ions undergoing competing dissociation should be characterized by two different temperatures rather than by a single "effective" temperature.[15] Drahos and Vékey have presented a detailed analysis of the meaning of the effective temperature.[13] They concluded that it is not a thermodynamic quantity and that it depends on the average internal energy of the ensemble of decomposing ions (not to the internal energy distribution in the ion source), the critical energy for fragmentation and the experimental time window. Surprisingly, they further found that T_{eff} approaches 0 K when the mean internal energy of fragmenting ions is close to the fragmentation threshold. Ervin derived an analytical expression for the effective temperature using classical RRK theory.[20] He found that the effective temperature is directly proportional to the average activation energy for cluster fragmentation, inversely proportional to the number of vibrational degrees of freedom in the cluster, and depends both on the time-window sampled experimentally and on the product of preexponential factors for the two competing reactions.

Finite heat bath theory (FHBT) developed by Klots[21−29] employs the steepest descent approximation[30] to calculate the microcanonical rate constant as a function of internal energy. This theory has been used to explore various aspects of unimolecular reaction dynamics. These include extracting fragmentation energetics from kinetic energy release distributions (KERDs);[31−36] exploring the influence of angular momentum,[23,24] excess internal energy and reaction threshold[24,27,28] on the microcanonical rate constant, and the branching ratio for competing reactions.[24,37] Until now FHBT has been most extensively used to study consecutive fragmentation of clusters and for quantifying magic numbers in cluster ion mass spectra.[25,26,33] Recent advances in applications of FHBT have been summarized in several reviews.[38,39] In the present work we use FHBT to provide a rigorous theoretical basis of the kinetic method and resolve remaining uncertainties on its general applicability and limitations.

FHBT Formalism

It is well known that a canonical rate constant, $k(T)$, can be obtained upon averaging of a microcanonical rate constant, $k(E)$,

over a thermal distribution of energies. Finite heat bath theory, alternatively called thermal kinetics in small systems, provides a simple analytical relationship between the two rate constants that is valid for all finite sizes of the energized medium (finite heat bath) and ensures that $k(E)$ would approach $k(T)$ as the system becomes large enough to serve its own heat bath (infinite heat bath).

FHBT uses the RRKM expression for the microcanonical rate constant

$$k(E) = \frac{\sigma W^{\ddagger}(E - E_0)}{h\rho(E)} \tag{7}$$

where $\rho(E)$ is the density of states of the reactant, $W^{\ddagger}(E - E_0)$ is the sum of states of the transition state, E_0 is the critical energy, h is Plank's constant, and σ is the reaction path degeneracy.

The transformation between the internal energy domain and the temperature domain is achieved using the first-order steepest descent approximation[30] to calculate the sums and densities of states (see Appendix of ref 27 for more details). The density of states of the reactant can be calculated using the steepest descent expression modified by Klots:[27]

$$\rho(E) = \frac{Q(T)\exp(E/k_{\mathrm{B}}T)}{k_{\mathrm{B}}T\sqrt{2\pi(C-1)}} \tag{8}$$

where $Q(T)$ is the partition function, k_{B} is the Boltzmann constant, and C is the heat capacity of the molecule evaluated at temperature T. The internal energy, E, and the temperature, T, are related through the following expression:[27]

$$E = \bar{E}(T) - k_{\mathrm{B}}T \tag{9}$$

where $\bar{E}(T)$ is the average energy of the reactant evaluated at temperature T.

The steepest-descent approximation provides a simple relationship between the sum and the density of states[30]

$$W(E) = k_{\mathrm{B}}T\rho(E) \tag{10}$$

where now E and T are related through eq 11

$$E = \bar{E}(T) \tag{11}$$

It can be concluded based on eqs 8 and 9 that the sum of states can be thought of as a density of states of a system with one additional vibrational degree of freedom. As a result, one has

$$W(E) = \frac{Q(T)\exp(E/k_{\mathrm{B}}T)}{\sqrt{2\pi(C-1)}} \tag{12}$$

The sum of states in the transition state, $W^{\ddagger}(E - E_0)$, characterized by internal energy $E - E_0$ and temperature $T^{\ddagger}$ can be written as

$$W^{\ddagger}(E - E_0) = \frac{Q^{\ddagger}(T^{\ddagger})\exp((E - E_0)/k_{\mathrm{B}}T^{\ddagger})}{\sqrt{2\pi C^{\ddagger}}} \tag{13}$$

where now

$$E - E_0 = \bar{E}^{\ddagger}(T^{\ddagger}) \tag{14}$$

and $\bar{E}^{\ddagger}(T^{\ddagger})$ is the average energy of the transition state evaluated at temperature $T^{\ddagger}$.

The microcanonical rate constant can be expressed as

$$k(E) = \frac{\sigma k_{\mathrm{B}}T}{h}\frac{Q^{\ddagger}(T^{\ddagger})}{Q(T)}\left(\frac{C-1}{C^{\ddagger}}\right)^{1/2}\frac{\mathrm{e}^{(E-E_0)/k_{\mathrm{B}}T^{\ddagger}}}{\mathrm{e}^{E/K_{\mathrm{B}}T}} \tag{15}$$

Branching Ratios

Replacing the critical energy E_0 with the critical energies ΔE_1 and ΔE_2 for reactions 2a and 2b, respectively in eq 15, the branching ratio, $k_1(E)/k_2(E)$, is given by

$$\frac{k_1(E)}{k_2(E)} = \frac{Q_1^{\ddagger}(T_1^{\ddagger})}{Q_2^{\ddagger}(T_2^{\ddagger})}\left(\frac{C_2^{\ddagger}}{C_1^{\ddagger}}\right)^{1/2}\frac{\mathrm{e}^{(E-\Delta E_1)/k_{\mathrm{B}}T_1^{\ddagger}}}{\mathrm{e}^{(E-\Delta E_2)/k_{\mathrm{B}}T_2^{\ddagger}}} \tag{16}$$

The logarithmic branching ratio, assuming that $C_1^{\ddagger} \approx C_2^{\ddagger}$, is

$$\mathrm{BR} \equiv \ln\frac{k_1(E)}{k_2(E)} = \ln\left(\frac{Q_1^{\ddagger}(T_1^{\ddagger})}{Q_2^{\ddagger}(T_2^{\ddagger})}\right) + E\left(\frac{1}{k_{\mathrm{B}}T_1^{\ddagger}} - \frac{1}{k_{\mathrm{B}}T_2^{\ddagger}}\right) - \frac{\Delta E_1}{k_{\mathrm{B}}T_1^{\ddagger}} + \frac{\Delta E_2}{k_{\mathrm{B}}T_2^{\ddagger}} \tag{17}$$

Equation 17 is perfectly general provided the steepest descent approximation is valid. Hoare and Ruijgrok have demonstrated that the accuracy of the first-order steepest descent approximation increases for larger molecules.[30] Comparison of steepest descent (SD) and direct count calculations for a small molecule with 15 vibrational degrees of freedom showed that SD sum of states is calculated with less than 5% error for internal energies above 0.1 eV.[40] However, according to Hoare and Ruijgrok,[30] the sum of states for cyclopropane ($N = 21$) for the excess internal energy of 10 kcal/mol (0.43 eV) calculated using the first-order steepest descent approximation is 10% lower than the value obtained using direct count. In this study we present simulation results for systems with more than 50 vibrational degrees of freedom, for which the steepest-descent approximation provides quite accurate results.

An interesting observation that emerges from eq 17 is that the slope of the plot of BR vs ΔE_2 (the kinetic plot) is given by $1/k_{\mathrm{B}}T_2^{\ddagger}$. It follows that the kinetic plot is linear only if $T_2^{\ddagger}$ is constant over the range of experimental conditions for which the branching ratios are measured. Note that the same result can be obtained using a basic theorem of FHBT[21]

$$\frac{\partial \ln k(E,E_0)}{\partial E_0} = -\frac{1}{k_{\mathrm{B}}T^{\ddagger}} \tag{18}$$

What is the physical meaning of the transition state temperature? Klots has shown that for reactions proceeding via a loose transition state, $T^{\ddagger}$ is characteristic of the kinetic energy distribution of departing fragments.[24,28] Even the fragmentation of a pure microcanonical ensemble results in formation of fragments with a distribution of kinetic energies. Thus the transition state temperature has a clear physical meaning regardless of the initial internal energy distribution of the ensemble of decomposing ions.

At this point it is interesting to examine two limiting cases, for which eq 17 simplifies to the commonly used kinetic method eq 3:

(1) Equation 3 is obtained from eq 17 if $T_1^{\ddagger} = T_2^{\ddagger}$. This will happen either in the trivial case where $\Delta E_1 = \Delta E_2$ or for an infinite heat bath, i.e., for very large ions or for ions having a

thermal distribution of energies. These limiting case conditions were not met in experiments where the kinetic method has been successfully used.

(2) Another limiting case arises when the internal energy of the reacting population is just above the fragmentation threshold for reaction 1; i.e., $E \approx \Delta E_1$. Substituting ΔE_1 for E in eq 17 yields eq 3. Thus the kinetic method should be successful for all reactions that exhibit a very small kinetic shift! However, it is not apparent whether the kinetic method would yield accurate results for larger systems, for which the kinetic shift is not negligible. We address this question in the simulations presented below.

RRKM and FHBT Calculations

RRKM and FHBT calculations were performed to address two questions: (1) Is the kinetic plot linear or, alternatively, is the transition state temperature, $T_2^{\ddagger}$ constant over a range of critical energies for reaction 2b (ΔE_2) typically sampled experimentally? (2) Will the kinetic method yield accurate thermochemical information for large molecules such as peptides?

Simulations were performed using the peptide frequency model developed by Griffin and McAdoo.[41] The results presented below were insensitive to the exact values of frequencies employed, and the conclusions are general independent of the frequency model used. To model transition states for reactions 2a and 2b, one frequency, 1200 cm^{-1}, was chosen to represent the reaction coordinate, and eight other frequencies in the range 100−1200 cm^{-1} were varied to yield the desired transition state entropy ($\Delta S^{\ddagger}$). Calculations were performed for molecular ions having 50,100, 150, 200, 300, and 500 vibrational degrees of freedom (DOF). Three different transition state models were used to represent the difference in transition state entropies for reactions 2a and 2b ($\Delta(\Delta S^{\ddagger}) = \Delta S_2^{\ddagger} - \Delta S_1^{\ddagger}$):

Model 1: $\Delta S_1^{\ddagger} = 6$ e.u. and $\Delta S_2^{\ddagger} =$ 6 e.u $\Rightarrow \Delta(\Delta S^{\ddagger}) = 0$ e.u.

Model 2: $\Delta S_1^{\ddagger} = 6$ e.u. and $\Delta S_2^{\ddagger} =$ 3 e.u $\Rightarrow \Delta(\Delta S^{\ddagger}) = -3$ e.u.

Model 3: $\Delta S_1^{\ddagger} = 6$ e.u. and $\Delta S_2^{\ddagger} =$ 9 e.u $\Rightarrow \Delta(\Delta S^{\ddagger}) = 3$ e.u.

The critical energy for reaction 2a (ΔE_1) was kept at a constant value of 1 eV, while ΔE_2 was changed in the range $\Delta E_1 - 0.1$ eV $< \Delta E_2 < \Delta E_1 + 0.1$ eV.

The simulation scheme was as follows:

(1) Calculate rate-energy dependencies for reactions 2a (k_1(E)) and 2b (k_2(E)).

(2) Calculate $\bar{E}_1^{\ddagger}(T^{\ddagger})$ and $\bar{E}_2^{\ddagger}(T^{\ddagger})$ based on the frequencies of the corresponding transition states ($\nu_i^{\ddagger}$):

$$\bar{E}^{\ddagger}(T^{\ddagger}) = \sum_{i=1}^{N} \frac{h\nu_i^{\ddagger}}{\exp(h\nu_i^{\ddagger}/k_B T^{\ddagger}) - 1} \qquad (19)$$

where N is the number of vibrational degrees of freedom in the transition state.

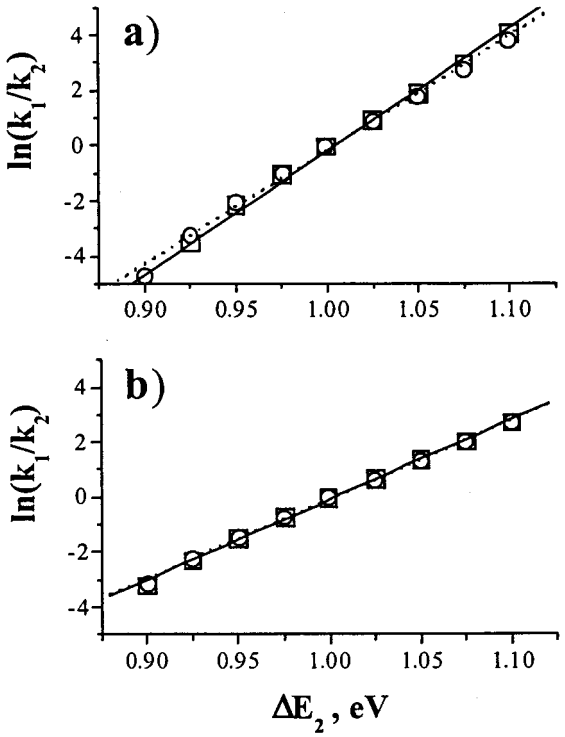

Figure 1. Kinetic plots obtained using RRKM (○) and FHBT (□) calculations for (a) $N = 50$ and (b) $N = 100$. The solid line corresponds to a linear fit of FHBT results, whereas the dotted line represents a linear fit of RRKM results.

(3) Find the internal energy (E_{mp}) that gives the most probable rate constant sampled experimentally (k_{mp}). For a system of two competing reactions, k_{mp} is given by:

$$k_{mp} = k_1(E_{mp}) + k_2(E_{mp}) \qquad (20)$$

The most probable rate constant is determined by the geometry of the mass spectrometer and by the type of experiment performed. For example, metastable decay in a mass spectrometer is characterized by a lower k_{mp} than is collision-induced dissociation (CID). Simulations were performed for the most probable rate constants of 5×10^4, 1×10^5, and 5×10^5 s^{-1} that represent, respectively, metastable and CID fragmentation at two different collision energies.

(4) Calculate $E_{mp} - \Delta E_1$ and $E_{mp} - \Delta E_2$ and find $T_1^{\ddagger}$ and $T_2^{\ddagger}$ using the known relationship between $E^{\ddagger}$ and $T^{\ddagger}$.

(5) Calculate $Q_1^{\ddagger}$ and $Q_2^{\ddagger}$ using eq 21

$$Q^{\ddagger}(T^{\ddagger}) = \prod_{i=1}^{N} \frac{1}{1 - \exp(-h\nu_i^{\ddagger}/k_B T^{\ddagger})} \qquad (21)$$

(6) Calculate $\ln(k_1/k_2)$ from eq 17.

Results and Discussion

Kinetic plots obtained from RRKM and FHBT calculations using Model 1 ($\Delta(\Delta S^{\ddagger}) = 0$), $k_{mp} = 1 \times 10^5$ s^{-1}, and $N = 50$ and 100 are shown in Figure 1a,b. Results obtained using FHBT are in fairly good agreement with RRKM calculations. For larger clusters ($N > 50$), the difference in branching ratios obtained using the two methods is less than 2%. The agreement between RRKM and FHBT calculations becomes somewhat worse when the excess energy above the fragmentation threshold is below 0.1 eV. The deviation probably results from the deficiency of the steepest descent approximation and is most apparent for

TABLE 1: Results of FHBT Simulations for $\Delta E_1 = 1$ eV; $\Delta E_2 = 1.1$ eV; $\Delta(\Delta S^{\ddagger}) = 0$; $k_{mp} = 1 \times 10^5$ s^{-1}

N	E_{mp}[a]	$E_{mp} - \Delta E_1$	$T_1^{\ddagger}$	$E_{mp} - \Delta E_2$	$T_2^{\ddagger}$	$E\left(\frac{1}{k_B T_1^{\ddagger}} - \frac{1}{k_B T_2^{\ddagger}}\right)$	$\ln\left(\frac{Q_1^{\ddagger}}{Q_2^{\ddagger}}\right)$	$\frac{\Delta E_1}{k_B T_1^{\ddagger}}$	$\frac{\Delta E_2}{k_B T_2^{\ddagger}}$	$\ln\left(\frac{k_1}{k_2}\right)$	$\Delta(\Delta E)_{max}$[b]
50	1.233	0.233	305.1	0.133	233.8	−14.29	1.98	38.00	54.55	4.24	0.1
100	1.837	0.837	421.6	0.737	394.8	−3.42	1.38	27.50	32.30	2.76	0.15
150	2.472	1.472	462.5	1.372	445.9	−2.31	1.27	25.07	28.60	2.49	0.17
200	3.106	2.106	482.1	2.006	470.1	−1.91	1.21	24.05	27.13	2.38	0.18
300	4.393	3.393	502.5	3.293	494.8	−1.59	1.16	23.07	25.78	2.28	0.19
500	6.985	5.985	519.3	5.885	514.8	−1.37	1.13	22.33	24.77	2.20	0.2

[a] All energies are in eV, all temperatures are in K. [b] For $N = 30$ $\Delta(\Delta E)_{max} = 0.002$ eV.

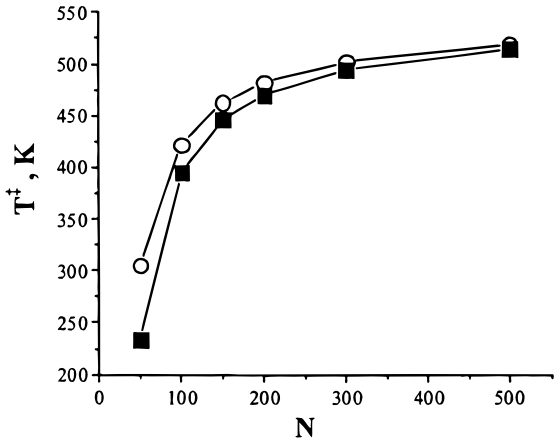

Figure 2. Dependence of $T_1^{\ddagger}$(○) and $T_2^{\ddagger}$(■) on the number of degrees of freedom in the cluster.

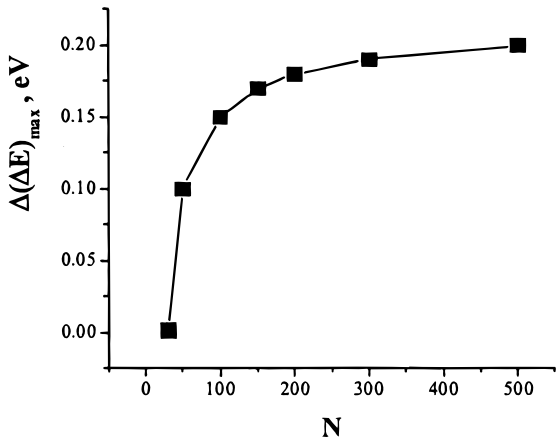

Figure 3. Maximum measurable difference in the critical energies for reactions 2a and 2b as a function of the number of degrees of freedom in the cluster.

$N = 50$ and low k_{mp} (5×10^4 s^{-1}). Nevertheless, both methods yield the same qualitative picture of fragmentation even for smaller clusters.

Typical output obtained from FHBT simulations for $\Delta E_1 = 1$ eV, $\Delta E_2 = 1.1$ eV, $\Delta(\Delta S^{\ddagger}) = 0$, $k_{mp} = 1 \times 10^5$ s^{-1} is summarized in Table 1. As expected, the most probable internal energy (E_{mp}) sampled experimentally rises linearly with the number of degrees of freedom in the molecular ion (N). An interesting result that follows from the data presented in Table 1 is that there are two distinct temperatures ($T_1^{\ddagger}$ and $T_2^{\ddagger}$) that characterize two reactions in competition. As mentioned earlier, Holmes and co-workers have proposed previously the existence of two different temperatures rather than one effective temperature characterizing competing reactions.[15] Figure 2 shows the dependence of the two transition state temperatures ($T_1^{\ddagger}$ and $T_2^{\ddagger}$) on N. A sharp rise in $T^{\ddagger}$ for small values of N is followed by a much slower increase for large N. This indicates that the transition state temperature is approaching asymptotically the value characteristic of an infinite heat bath as the molecular ion becomes large. Moreover, with increase in the number of degrees of freedom, $T_1^{\ddagger}$ and $T_2^{\ddagger}$ approach each other. The difference between $T_1^{\ddagger}$ and $T_2^{\ddagger}$ is about 30% for $N = 50$, less than 7% for $N = 100$, and decreases to about 1% for $N = 500$. In this example $T_1^{\ddagger}$ is greater than $T_2^{\ddagger}$ for all values of N. This is because the critical energy for reaction 2b (ΔE_2) is higher than ΔE_1 and, as a result, the excess internal energy for reaction 2b is always smaller than the excess internal energy for reaction 2a.

The last column in Table 1 corresponds to a maximum value for the difference in the critical energies for reactions 2a and 2b that can be observed experimentally, $\Delta(\Delta E)_{max}$. We defined $\Delta(\Delta E)_{max}$ as the difference in critical energies for reactions 2a and 2b that would give rise to a formation of 1% of B_2H^+ (fragmentation following reaction 2b) and 99% of B_1H^+ (fragmentation following reaction 2a). For small systems the value of $\Delta(\Delta E)_{max}$ is low. For example, $\Delta(\Delta E)_{max} = 0.002$ for $N = 30$. Since microcanonical rate constants rise sharply with internal energy for relatively small clusters, two competing reactions can be observed simultaneously only in a very narrow range of $\Delta(\Delta E)_{max}$. For larger ions, however, microcanonical rate constants rise much slower with internal energies. As a result, a broader range of $\Delta(\Delta E)$s can be sampled experimentally (see Figure 3).

Kinetic plots were created for the three different transition state models described in the previous section. The values of BR covered the range between −4.5, corresponding to $B_1H^+/B_2H^+ = 0.011$, and 4.5, corresponding to $B_1H^+/B_2H^+ = 90$. The critical energy for reaction 2a, ΔE_1, and the difference in the transition state entropies for reactions 2a and 2b, $\Delta(\Delta S^{\ddagger})$, were extracted from the kinetic plots using the extended version of the kinetic method (equations 5 and 6). The results obtained using FHBT and RRKM calculations are summarized in Table 2. Effective temperatures (T_{eff}) determined from the slopes of the kinetic plots will be considered later in this section. The critical energy obtained from the simulations is in remarkably good agreement with the input value of 1 eV for ΔE_1. For all cases examined in the simulations, the deviation between the calculated and the correct value is less than 3%. The deviation in proton affinity (data not shown) from the assumed value of 230 kcal/mol was found to be less than 1 kcal/mol. *These results demonstrate that high-quality thermochemical information can be obtained using the extended version of the kinetic method for any cluster size, provided both competing reactions have negligible reverse activation barriers.*

The values of $\Delta(\Delta S^{\ddagger})$ are also in a good agreement with the differences in the transition state entropies assumed in the modeling. The reason for a larger deviation of $\Delta(\Delta S^{\ddagger})$ obtained from FHBT calculations for $N = 50$ will become clear from the following considerations. A closer examination of the kinetic

TABLE 2: Binding Energy for Reaction 2a and the Entropy Difference Obtained from Calculated Kinetic Plots Using the Extended Version of the Kinetic Method[7−9]

	Model 1				Model 2				Model 3			
	FHBT		RRKM		FHBT		RRKM		FHBT		RRKM	
N	ΔE_1	$\Delta(\Delta S^{\ddagger})$	ΔE_1	$\Delta(\Delta S^{\ddagger})$	ΔE_1	$\Delta(\Delta S^{\ddagger})$	ΔE_1	$\Delta(\Delta S^{\ddagger})$	ΔE_1	$\Delta(\Delta S^{\ddagger})$	ΔE_1	$\Delta(\Delta S^{\ddagger})$
50	0.999	0.29	1.004	−0.13	1.008	−1.86	1.013	−2.43	1.003	1.53	0.992	2.74
100	1.003	0.11	1.004	0.01	1.019	−2.39	1.017	−2.65	0.987	2.68	0.984	3.12
150	1.001	0.18	0.999	0.27	1.023	−2.56	1.021	−2.74	0.981	2.97	0.980	3.34
200	1.003	0.18	1.000	0.32	1.026	−2.66	1.021	−2.76	0.990	2.51	0.989	2.85
300	1.002	0.19	0.999	0.32	1.027	−2.72	1.021	−2.77	0.988	2.62	0.988	2.90
500	1.001	0.22	0.998	0.34	1.028	−2.78	1.022	−2.78	0.985	2.71	0.987	2.94

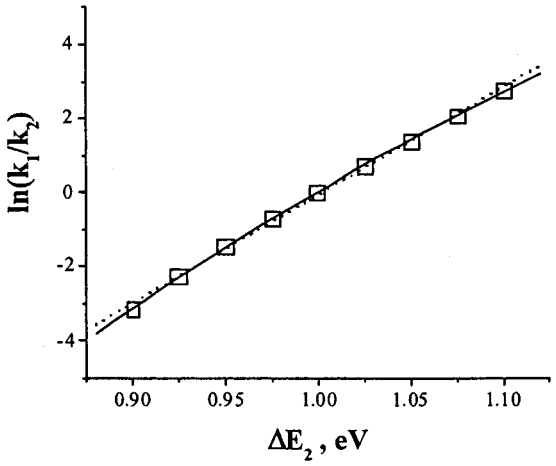

Figure 4. Second-order polynomial fit (solid line) and a linear fit (dotted line) to the kinetic plot obtained using Model 1, $k_{mp} = 1 \times 10^5$ s^{-1} and $N = 100$.

plots shown in Figure 1 reveals that, although the kinetic plots are well approximated by straight lines, the points systematically deviate from the corresponding linear fits. Figure 4 shows the kinetic plot for N = 100 with a linear and second-order polynomial fits. Although the linear regression presented in the figure shows a reasonable agreement with the results of simulations, the polynomial fit shows a better correlation with the data points. RRKM calculations performed using both Whitten−Rabinovitch semiclassical approximation[42] and direct count Beyer−Swinehart algorithm[42] confirmed that, regardless of the approach used to calculate the microcanonical rate constants, the kinetic plots show a nonlinear behavior. It should be mentioned also that the curvature of the kinetic plots has been previously pointed out by Ervin[20] based on RRK calculations. In the present work we found that the curvature of the calculated kinetic plots could increase substantially when lower level approximations are used to calculate the sums and densities of states. It was apparent that the steepest descent approximation provided much lower quality results for $N = 50$ and lower reaction rate constants than the Whitten−Rabinovitch or direct count procedures. Since RRK is incapable of providing correct rate constants even within an order of magnitude[40] we expect that the results of RRK calculations will strongly overestimate the curvature.

Since the slope of the kinetic plot is given by $1/k_B T_2^{\ddagger}$, examining the behavior of the transition state temperature for reaction 2b ($T_2^{\ddagger}$) provides a better understanding of the origin of the observed curvature of the kinetic plot. The dependence of $T_2^{\ddagger}/T_{eff}$ on the critical energy for reaction 2b (ΔE_2) obtained using Model 1 and $k_{mp} = 1 \times 10^5$ s^{-1} is shown in Figure 5. It is clear that the transition state temperature is not constant over the range of critical energies for reaction 2b examined in the simulations. Following the increase in ΔE_2, $T_2^{\ddagger}$ first increases, then passes through a maximum and drops down. The maximum

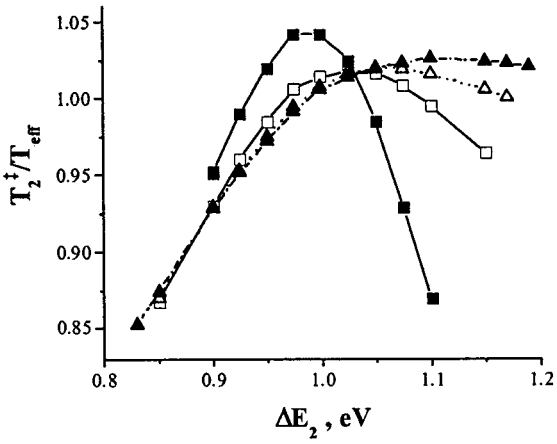

Figure 5. Reduced transition state temperature for reaction 2b as a function of ΔE_2 for Model 1 and $k_{mp} = 1 \times 10^5$ s^{-1}; (■) $N = 50$, (□) $N = 100$, (△) $N = 200$, and (▲) $N = 500$.

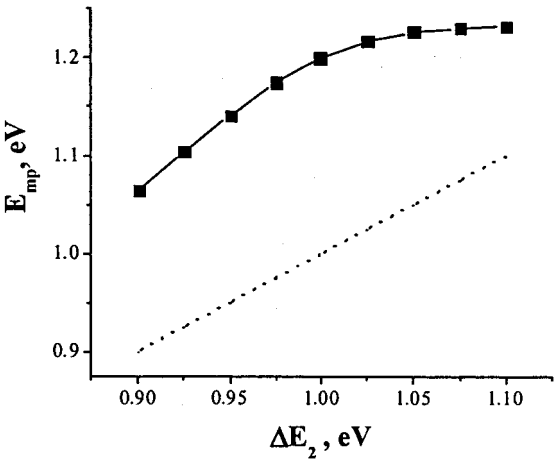

Figure 6. Most probable energy giving rise to the most probable rate constant of 1×10^5 s^{-1} for $N = 50$ (■, −). The dotted line shows the change is ΔE_2.

is much more pronounced for smaller size clusters and is only barely distinguished for $N = 500$.

What are the factors that govern this peculiar behavior of $T_2^{\ddagger}$? The transition state temperature is derived from the difference between the most probable internal energy for a system of competing reactions and the reaction threshold. Figure 6 shows the change of E_{mp} as a function of ΔE_2 for Model 1 and $k_{mp} = 1 \times 10^5$ s^{-1}. The most probable energy rises are with increase in ΔE_2 in the range of critical energies where reaction 2b either dominates or competes efficiently with reaction 2a. However, when ΔE_2 becomes greater than ΔE_1 and reaction 2a becomes dominant, E_{mp} levels off to the value of the kinetic shift for reaction 2a. The dashed line in Figure 6 represents the change in ΔE_2 (slope = 1). The difference between E_{mp} and ΔE_2 will increase for small values of ΔE_2

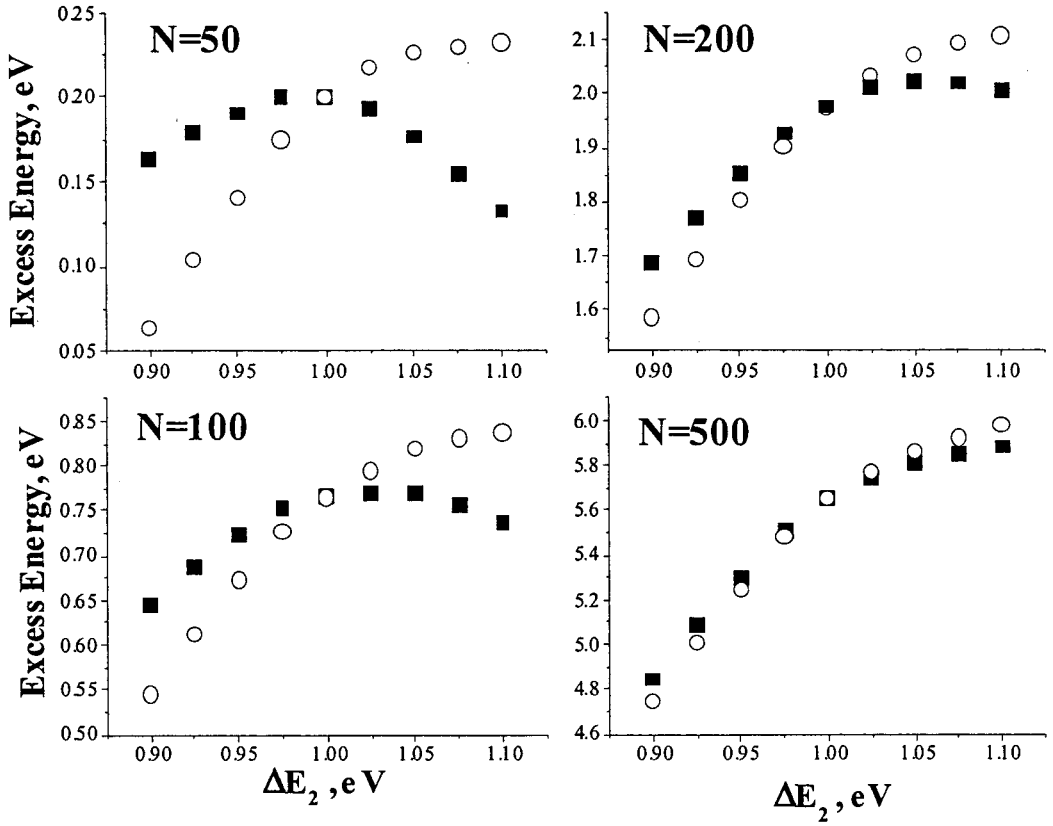

Figure 7. Excess internal energy for reactions 2a (○) and 2b (■) as a function of ΔE_2 for different values of N.

TABLE 3: Comparison between the Average Value for $T_2^{\ddagger}$ and the Effective Temperature (T_{eff}) Obtained from Kinetic Plots

	Model 1				Model 2				Model 3			
	$k_{mp} = 5 \times 10^4\ s^{-1}$		$k_{mp} = 5 \times 10^5\ s^{-1}$		$k_{mp} = 5 \times 10^4\ s^{-1}$		$k_{mp} = 5 \times 10^5\ s^{-1}$		$k_{mp} = 5 \times 10^4\ s^{-1}$		$k_{mp} = 5 \times 10^5\ s^{-1}$	
N	$T_2^{\ddagger}$	T_{eff}	$T_2^{\ddagger}$	T_{eff}	$T_2^{\ddagger}$	T_{eff}	$T_2^{\ddagger}$	T_{eff}	$T_2^{\ddagger}$	T_{eff}	$T_2^{\ddagger}$	T_{eff}
50	244.2	242.8	318.4	317.9	262.9	256.7	341.4	346.2	224.5	232.1	290.8	317.9
100	370.2	363.5	436.5	430.1	386.4	367.8	456.1	439.5	354.9	375.4	416.5	436.8
150	414.6	412.2	478.5	480.1	427.7	419.5	494.7	486.8	400.1	416.7	457.9	477.7
200	437.4	429.9	494.5	487.0	444.9	427.0	509.7	491.7	421.1	438.1	480.6	500.8
300	460.6	454.0	515.7	509.1	466.0	450.0	529.0	512.1	445.4	462.6	503.4	523.3
500	479.2	473.2	532.5	526.3	483.0	468.2	544.5	528.2	464.8	481.7	521.3	541.3

since the slope of E_{mp} vs ΔE_2 is greater than unity. However, at some point along the curve, the slope of E_{mp} vs ΔE_2 becomes smaller than unity and, as a result, $E_{mp} - \Delta E_2$ decreases. In contrast, since ΔE_1 is constant, the transition state temperature for reaction 2a ($T_1^{\ddagger}$) will show a different behavior. We expect $E_{mp} - \Delta E_1$ and $T_1^{\ddagger}$ to increase steadily with increase in ΔE_2. The change in the excess internal energy for reactions 2a (E_1^{exc}) and 2b (E_2^{exc}) as a function of ΔE_2 for different cluster sizes is presented in Figure 7. While for small clusters there is a substantial difference between E_1^{exc} and E_2^{exc}, the excess energies almost overlap for $N = 500$. *This clearly demonstrates that a single temperature can effectively characterize fragmentation of large clusters*.

Why is the slope of E_{mp} vs ΔE_2 greater than unity? Klots has shown that the slope of the plot of E_{mp} vs ΔE_2 is given by[27]

$$\left(\frac{\partial E}{\partial \Delta E}\right)_k = \frac{T}{T - T^{\ddagger}} \tag{22}$$

where the right-hand side is a so-called Carnot−Kelvin factor. This factor is, of course, greater than unity. As a result, small variations in the reaction threshold can lead to a much more prominent change in the internal energy needed to maintain a most probable rate constant characteristic of a particular experimental setup. For relatively small clusters, for which $T^{\ddagger}$ is much smaller than T, the Carnot−Kelvin factor is close to unity and the amplification effect is not very marked. However, when the transition state temperature becomes comparable with T, this factor can be much greater than unity. It is clear now that because for large clusters the most probable energy changes much faster than ΔE_2 (ΔE_2 becomes effectively constant compared to E_{mp}), the behavior of $T_2^{\ddagger}$ is mainly determined by E_{mp}. As a result, the plot of $T_2^{\ddagger}$ vs ΔE_2 for $N = 500$ does not exhibit a pronounced maximum (see Figure 5).

Table 3 shows a comparison of the average values of $T_2^{\ddagger}$ with the "effective" temperatures derived from linear fits of the kinetic plots. The deviation between the average transition state temperature and the effective temperature is less than 5% in most of the cases. It follows that the effective temperature derived from the kinetic plot closely resembles the average transition state temperature for reaction 2b. It also follows from the above discussion that the "effective" temperature is indeed a semiempirical parameter.[15] However, the correspondence between the effective temperature and the average value of the transition state temperature allows us to attribute some meaning to the former. Thus we conclude that it is a good approximation

to assign the effective temperature to the transition state temperature for reaction 2b. More important, T_{eff} shows the same behavior as the transition state temperature as a function of various experimental parameters. One would expect that T_{eff} (1) is correlated with the average energy of the reacting population (E_{mp}) through the average excess internal energy $E_{mp} - <\Delta E_2>$; (2) is independent of the temperature of the ion source as long as the latter is high enough to maintain an initial energy distribution much wider than the internal energy distribution of the population of reacting ions; (3) approaches zero at reaction threshold (in agreement with the results of RRKM calculations by Drahos and Vékey[13] that showed that the "effective" temperature approaches zero at the reaction threshold); (4) decreases with increasing the reaction time sampled experimentally; and (5) rises with increasing cluster size. Drahos and Vékey[13] and Ervin[20] have drawn some of these conclusions previously. However, the microscopic analysis bared upon FHBT we have just presented provides a more general rational for these conclusions.

The above definition of the effective temperature should be contrasted with a definition given by Drahos and Vékey.[13] These authors define the effective temperature as a temperature characteristic of a canonical ensemble that would give the same branching ratio as observed experimentally. This definition closely resembles the definition of the so-called bath temperature (T_b) commonly used in FHBT. However, the temperature defined in this way relates to the energy of the energized ion ($\overline{E}$) rather than to the excess internal energy above the fragmentation threshold ($\overline{E}^{\ddagger}$) that determines the transition state temperature. In contrast, our formulation demonstrates that the effective temperature is a good measure of the average transition state temperature for reaction, which depends on the *excess* internal energy above the fragmentation threshold rather than on the *total* internal excitation of the ion.

Obtaining Relative Reaction Energetics from Kinetic Energy Release Measurements. It can be shown using FHBT that the microcanonical rate constant is given by the following expression:[21,38]

$$k(E) = \frac{e k_B T}{h} e^{\Delta S^{\ddagger}/k_B} \left(\frac{T^{\ddagger}}{T}\right)^C \tag{23}$$

where C is the heat capacity of the energized ion. The branching ratio is then given by

$$\frac{k_1}{k_2} = e^{\Delta(\Delta S^{\ddagger})/k_B} \left(\frac{T_1^{\ddagger}}{T_2^{\ddagger}}\right)^C \tag{24}$$

and therefore

$$\ln\left(\frac{k_1}{k_2}\right) = \frac{\Delta(\Delta S^{\ddagger})}{k_B} + C \ln\left(\frac{T_1^{\ddagger}}{T_2^{\ddagger}}\right) \tag{25}$$

Furthermore, from eq 14 one obtains

$$\Delta E_2 - \Delta E_1 = \overline{E}_1^{\ddagger}(T_1^{\ddagger}) - \overline{E}_2^{\ddagger}(T_2^{\ddagger}) \tag{26}$$

Equation 26 demonstrates that measuring the transition state temperatures for the competing reactions would yield the difference in critical energies for reactions 2a and 2b, $\Delta(\Delta E)$, and eq 25 allows to obtain the difference in the activation entropies from the measured branching ratio.

The transition state temperature can be derived from the kinetic energy release measurements. The kinetic energy release distribution (KERD) can be represented by[26,35]

$$P(\epsilon) = \epsilon^l \exp(-\epsilon/k_B T^{\ddagger}) \tag{27}$$

where l is a parameter ($0 < l < 1$). Fitting the experimental KERD with the above function will yield the transition state temperature for reaction. The combination of eqs 23−27 provides the most general approach for deducing the relative energetics and dynamics for competing reactions using the kinetic method. This is an important consideration for complex molecules, for which entropic factors are likely complications.

Conclusions

In the present work we have shown that the rigorous theoretical basis of the kinetic method can be obtained using finite heat bath theory (FHBT). A simple expression for the branching ratio has been derived (eq 17). For a microcanonical ensemble of ions, this expression can be simplified to eq 5, commonly used in the applications of the kinetic method, provided reaction 2a has a negligible kinetic shift or provided the ion of interest is large enough to serve as its own infinite heat bath. In all other cases, two different temperatures characterize competitive decay of a cluster: $T_1^{\ddagger}$ describing reaction 2a and $T_2^{\ddagger}$ describing reaction 2b. FHBT simulations confirm that, for large enough clusters, these two temperatures approach each other.

According to eq 17, $1/k_B T_2^{\ddagger}$ gives the slope of the kinetic plot. It follows that a necessary condition for linearity of the kinetic plot is that $T_2^{\ddagger}$ is constant over a range of critical energies for reaction 2b (ΔE_2) sampled experimentally. We have shown that $T_2^{\ddagger}$ actually changes with ΔE_2. Consequently, the kinetic plot is not linear, but can be well approximated by a straight line. The curvature of the kinetic plot is more pronounced for smaller clusters and lower reaction rate constants. Nevertheless, our results show that the kinetic method is capable of providing the relative binding energy for both small and large clusters with less than 3% error. It should be noted that relative transition state entropies determined using the extended version of the kinetic method are in reasonably good agreement with the input values used in our simulations.

Although the relative energetics for two competing reactions can be obtained with very high accuracy, care should be taken in deriving thermochemical data using the kinetic method. For example, protonated peptide can rearrange to a more stable structure through intramolecular hydrogen bonding. If this occurs, elimination of a peptide molecule from a proton-bound dimer can be associated with a nonnegligible reverse activation barrier. If reaction 2a has substantial reverse activation energy, the kinetic method necessarily overestimates the reaction thermochemistry.

Measurement of the kinetic energy release upon fragmentation provides an experimental measure of the degree of tightness or looseness of the reaction transition state and should be used to confirm the applicability of the kinetic method to a particular system. In the present work we proposed an approach for obtaining both the relative energetics and dynamics of two competing reactions from kinetic energy release distributions (KERDs). An advantage of the proposed approach is that it requires only relative measurements of a compound with unknown proton affinity vs a *single* reference base. It is our intention to test the accuracy of this method experimentally by carrying out a systematic study of collision-induced and metastable decay of proton-bound peptide dimers over a range of proton affinities and reaction times.

Acknowledgment. We gratefully acknowledge Professor Chava Lifshitz for very helpful discussions. This research was conducted under the auspices of the Office of Basic Energy Sciences, U.S. Department of Energy, under Contract DE-AC06-76RLO 1830 with the Battelle Memorial Institute, which operates the Pacific Northwest National Laboratory, a multi-program national laboratory operated from the Department of Energy.

References and Notes

(1) Cooks, R. G.; Patrick, J. S.; Kotiaho, T.; McLuckey, S. A. *Mass Spectrom. Rev.* **1994**, *13*, 287.
(2) Harrison, A. G. *Mass Spectrom. Rev.* **1997**, *16*, 201 and references therein.
(3) Cooks, R. G.; Wong, P. S. H. *Acc. Chem. Res.* **1998**, *31*, 379.
(4) Armentrout, P. B. J. Mass Spectrom. **1999**, *34*, 74.
(5) Cooks, R. G.; Kruger, T. L. *J. Am. Chem. Soc.* **1977**, *99*, 1279.
(6) McLuckey, S. A.; Cameron, D.; Cooks, R. G. *J. Am. Chem. Soc.* **1981**, *103*, 1313.
(7) Wu, Z.; Fenselau, C. *J. Am. Soc. Mass Spectrom.* **1992**, *3*, 863.
(8) Cheng, X.; Wu, Z.; Fenselau, C. *J. Am. Chem. Soc.* **1993**, *115*, 4844.
(9) Wu, Z.; Fenselau, C. *Rapid Commun. Mass Spectrom.* **1994**, *8*, 777.
(10) Cerda, B. A.; Wesdemiotis, C. *J. Am. Chem. Soc.* **1996**, *118*, 11884.
(11) Cerda, B. A.; Hoyau, S.; Ohanessian, G.; Wesdemiotis, C. *J. Am. Chem. Soc.* **1998**, *120*, 2437.
(12) Nold, M. J.; Cerda, B. A.; Wesdemiotis, C. *J. Am. Soc. Mass Spectrom.* **1999**, *10*, 1.
(13) Drahos, L.; Vékey, K. *J. Mass Spectrom.* **1999**, *34*, 79.
(14) Cooks, R. G.; Koskinen, J. T.; Thomas, P. D. *J. Mass Spectrom.* **1999**, *34*, 85.
(15) Holmes, J. L.; Aurby, C.; Mayer, P. M. *J. Phys. Chem. A* **1999**, *103*, 705.
(16) Cao, J.; Holmes, J. L. *Int. J. Mass Spectrom.* **2000**, *195*/*196*, 525.
(17) Thomas, P. D.; Cooks, R. G. *J. Phys. Chem. A* **2000**, *104*, 1359.
(18) Bojesen, G.; Breindahl, T. *J. Chem. Soc., Perkin Trans.* **1994**, *2*, 1029.
(19) Craig, S. L.; Zhong, M.; Choo, B.; Brauman, J. I. *J. Phys. Chem. A* **1997**, *101*, 19.
(20) Ervin, K. M. *Int. J. Mass Spectrom.* **2000**, *195*/*196*, 271.
(21) Klots, C. E. *J. Chem. Phys.* **1989**, *90*, 4470.
(22) Klots, C. E. *J. Chem. Phys.* **1990**, *93*, 4470.
(23) Klots, C. E. *J. Chem. Phys.* **1993**, *98*, 206.
(24) Klots, C. E. *J. Phys. Chem.* **1995**, *99*, 1748.
(25) Klots, C. E. *Z. Phys. D* **1991**, *20*, 105.
(26) Klots, C. E. *Z. Phys. D* **1991**, *21*, 335.
(27) Klots, C. E. *Int. Rev. Phys. Chem.* **1996**, *15*, 205.
(28) Klots, C. E. In *Unimolecular and Bimolecular Reaction Dynamics*; Ng, C. Y., Baer, T., Powis, I., Eds.; John Wiley & Sons Ltd: 1994.
(29) Lifshitz, C. *Int. J. Mass Spectrom. Ion Processes* **1992**, *118*/*119*, 315.
(30) Hoare, M. R.; Ruijgrok, Th. W. *J. Chem. Phys.***1970**, *52*, 113.
(31) Klots, C. E. *J. Chem. Phys.* **1993**, *98*, 1110.
(32) Klots, C. E. *J. Chem. Phys.* **1994**, *100*, 1035.
(33) Lifshitz, C.; Louage, F. *Int. J. Mass Spectrom. Ion Processes* **1990**, *101*, 101.
(34) Sandler, P.; Lifshitz, C.; Klots, C. E. *Chem. Phys. Lett.* **1992**, *200*, 445.
(35) Sandler, P.; Peres, T.; Weissman, G.; Lifshitz, C. *Ber. Bunsen-Ges. Phys. Chem.* **1992**, *96*, 1195.
(36) Laskin, J.; Peres, T.; Khong, A.; Jiménez-Vázquez, H. A.; Cross, R. J.; Saunders, M.; Bethune, D. S.; de Vries, M. S.; Lifshitz, C. *Int. J. Mass Spectrom. Ion Processes* **1999**, *185*/*186*/*187*, 61.
(37) Klots, C. E. *J. Phys. Chem. A* **1997**, *101*, 5378.
(38) Lifshitz, C. In *Cluster Ions*; Ng, C. Y., Baer, T., Eds.; John Wiley & Sons: New York, 1993.
(39) Lifshitz, C. In: *Current Topics in Ion Chemistry and Physics: Clusters*; Baer, T., Ng, T. C., Powis, I., Eds.; John Wiley & Sons: New York, 1993.
(40) Baer, T.; Hase, W. L. *Unimolecular Reaction Dynamics: Theory and Experiments*; Oxford University Press: New York, 1996.
(41) Griffin, L. L.; McAdoo, D. J. *J. Am. Soc. Mass Spectrom.* **1993**, *4*, 11.
(42) Holbrook, K. A.; Pilling, M. J.; Robertson S. H. *Unimolecular Reactions*; John Wiley & Sons: New York, 1996.